AGU PUBLICATIONS

Space Weather

RESEARCH ARTICLE

10.1002/2017SW001615

Testing nowcasts of the ionospheric convection from the expanding and contracting polar cap model

M.-T. Walach[1,2], S. E. Milan[1], T. K. Yeoman[1], B. A. Hubert[3], and M. R. Hairston[4]

[1]Department of Physics and Astronomy, University of Leicester, Leicester, UK, [2]Now at Department of Physics, Lancaster University, Lancaster, UK, [3]Laboratoire de Physique Atmosphérique et Planétaire, University of Liège, Liège, Belgium, [4]William B. Hanson Center for Space Sciences, University of Texas at Dallas, Richardson, Texas, USA

Key Points:
- A physics-based model of the expanding/contracting polar cap is used to calculate ionospheric convection, which is compared to measurements
- Flow velocity measurements stem from the cross-track ion drift meters on board DMSP satellites (in situ) and SuperDARN (ground based)
- Aside from small scale variations and dusk-dawn asymmetries, the model predicts directions and variation in magnitudes of the flows well

Correspondence to:
M.-T. Walach,
m.walach@lancaster.ac.uk

Citation:
Walach, M.-T., S. E. Milan, T. K. Yeoman, B. A. Hubert, and M. R. Hairston (2017), Testing nowcasts of the ionospheric convection from the expanding and contracting polar cap model, *Space Weather*, *15*, doi:10.1002/2017SW001615.

Received 22 FEB 2017
Accepted 31 MAR 2017
Accepted article online 6 APR 2017

Abstract The expanding/contracting polar cap (ECPC) model, or the time-dependent Dungey cycle, provides a theoretical framework for understanding solar wind-magnetosphere-ionosphere coupling. The ECPC describes the relationship between magnetopause reconnection and substorm growth phase, magnetotail reconnection and substorm expansion phase, associated changes in auroral morphology, and ionospheric convective motions. Despite the many successes of the model, there has yet to be a rigorous test of the predictions or nowcasts made regarding ionospheric convection, which remains a final hurdle for the validation of the ECPC. In this study we undertake a comparison of ionospheric convection, as measured in situ by ion drift meters on board DMSP (Defense Meteorological Satellite Program) satellites and from the ground by SuperDARN (Super Dual Auroral Radar Network), with motions nowcasted by a theoretical model. The model is coupled to measurements of changes in the size of the polar cap made using global auroral imagery from the IMAGE FUV (Imager for Magnetopause to Aurora Global Exploration Far Ultraviolet) instrument, as well as the dayside reconnection rate, estimated using the OMNI data set. The results show that we can largely nowcast the magnitudes of ionospheric convection flows using the context of our understanding of magnetic reconnection at the magnetopause and in the magnetotail.

Plain Language Summary We test a physics-based model which describes flows in the ionosphere near the magnetic poles due to solar wind driving of the activity within the Earth's magnetic environment using spacecraft and radar measurements of the flows. The results of this comparison show that our knowledge of the interactions of the solar wind, the Earth's magnetic environment, and ionosphere encompasses the general pattern of flows well, as well as the flow strengths. Further work is required to expand our understanding of asymmetric flows and to be able to model them better.

1. Introduction

Providing a framework for our current understanding, *Siscoe and Huang* [1985], *Freeman and Southwood* [1988], *Cowley and Lockwood* [1992], and *Lockwood and Cowley* [1992] established the expanding and contracting polar cap model (ECPC). The basis of this framework is as follows: the Earth's magnetic field within the polar cap is open and the polar cap size or open magnetic flux content is governed by dayside and nightside reconnection rates. At the nose of the magnetosphere, dayside reconnection opens flux during southward IMF by reconnecting the Earth's magnetic field with the interplanetary magnetic field (IMF), whereas nightside reconnection closes flux by reconnecting open flux from the Northern and Southern Hemispheres in the neutral sheet of the magnetotail. *Dungey* [1963] laid out the basis for this framework: opened field lines are stretched antisunward, across the polar cap, adding flux into the tail, where it can reconnect. This reconnected flux then convects back to the dayside via lower latitudes. The open magnetospheric flux, F_{PC}, thus varies with the dayside and nightside reconnection rates, Φ_D and Φ_N, through the following statement of Faraday's law:

$$\frac{dF_{PC}(t)}{dt} = \Phi_D(t) - \Phi_N(t) \quad (1)$$

(see *Milan* [2013], for more details).

As a result of the solar wind-driven magnetic flux convection, the flow pattern of plasma observed in the ionosphere is a twin-cell convection pattern, with the foci at the open-closed boundary near dusk and dawn

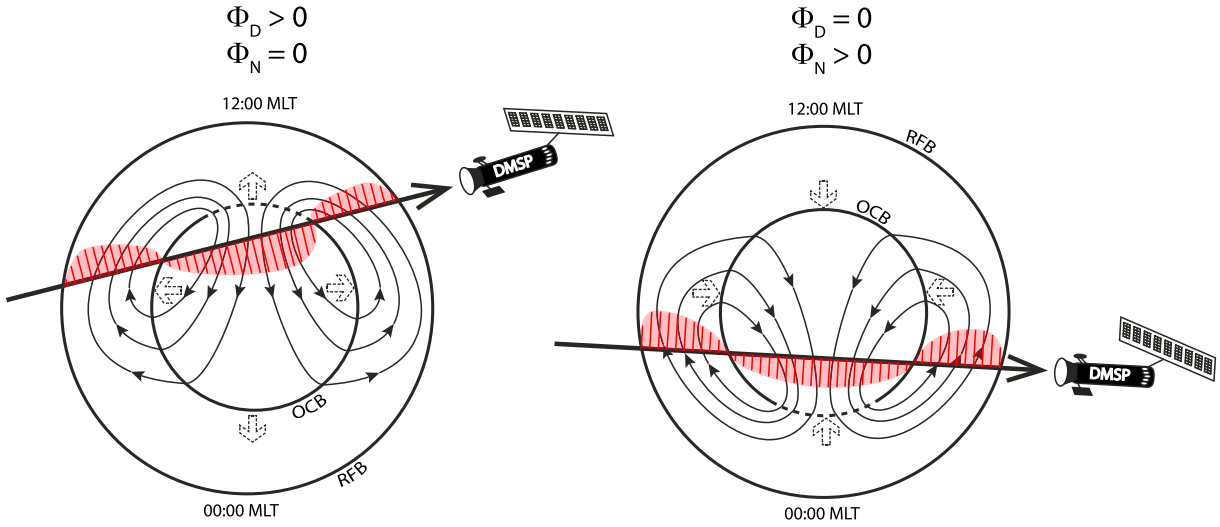

Figure 1. Schematics showing the polar cap convection, adapted from *Cowley and Lockwood* [1992] and *Lockwood and Cowley* [1992]. The schematics show the effects of (left) dayside and (right) nightside reconnection, respectively. The black arrows indicate the resulting ionospheric flows, and the flow lines are equivalent to the locations of the equipotentials. The dashed arrows indicate the expansion and contraction of the polar cap, resulting from reconnection. The dashed part of the open-closed field line boundary (OCB) indicates the location of the merging gaps. The lines in red indicate the expected velocities measured by the cross-track ion drift meter on board the DMSP satellites for a hypothetical satellite path, indicated by the thick black line. The outer circle indicates where the return flow boundary (RFB) is.

(as discussed by *Stern* [1975], *Heppner* [1977], *Volland* [1978], *Heppner and Maynard* [1987], *Foster* [1983], *Cowley and Lockwood* [1992, 1996], *Ruohoniemi and Greenwald* [1998], and others). The aim of this paper is to test the current understanding of the ECPC on a case study basis, using quantitative measurements of ionospheric flow velocities.

Figure 1 presents a schematic of the ionospheric flows when dayside (left) or nightside (right) reconnection dominates. In the former case the polar cap expands, and flow crosses the dayside merging gap. In the latter case flows cross the nightside merging gap and the polar cap contracts. The flow in the ionosphere is incompressible leading to interchange motions or return flows at lower latitudes. The plasma flows in the ionosphere are shown by black arrows, whereas the large dashed arrows indicate the expansion/contraction of the open-closed field line boundary (OCB). The red arrows indicate the measurements that a cross-track ion drift meter on a DMSP spacecraft would take.

Substorms and steady magnetospheric convection events are features which can be described by the expanding and contracting polar cap model, as, for example, discussed in *Walach and Milan* [2015]. *Lockwood et al.* [2009] also studied the ionospheric convection strengths using the Defense Meteorological Satellite Programme (DMSP) ion drift meter data. They considered a data set spanning all of 2001 and classified each pass by activity level (substorm phase or steady convection) using the *AE* indices. The findings of *Lockwood et al.* [2009] showed that the dayside and nightside reconnection rates can always be found to contribute to the cross polar cap potential (CPCP), but the probability of detecting the contribution of the driving varies between >99% during growth phases, 97% during quiet intervals, and 27% during steady convection events for Φ_D. For Φ_N the probability of detecting a contribution to the potential is highest during steady magnetospheric convection (>99%), whereas it is lower during the expansion (89%) or the recovery (96%) phases of a substorm.

Grocott et al. [2002, 2003] used SuperDARN data to observe flows in the polar ionosphere during substorms and steady convection. They observed large scale flows and expansions and contractions of the polar cap, fitting our understanding of the ECPC. Using mathematical formulae, based on equation (1), they estimated lower and upper limits on Φ_D and Φ_N, as well as the proportion of the open-closed field line boundary occupied by the merging gap from reconnection-driven ionospheric flows. Their finding was that during one interval of bursty nightside reconnection, Φ_N exceeded Φ_D by ~50%, whereas the nonburst-related Φ_N is of similar size as Φ_D. As the bursty flows they observed were not concurrent with any substorm phenomena, they concluded that the reconnection may be different from the classic Dungey cycle-related flows and be

occurring farther downtail. In this study the precise location of the reconnection site does not influence our results, as we are only concerned with the amount of reconnection occurring. Furthermore, we treat Φ_D and Φ_N as independent in the sense that they are linked via F_{PC} but occur independently of each other.

The results of studies by *Lockwood et al.* [2009] and *Grocott et al.* [2002, 2003], like many others, used the ECPC as a context to explain aspects of the magnetosphere-ionosphere coupling and dynamics. Although the ECPC is well understood and the framework has been shown to fit many observations, the relationship between Φ_D, Φ_N, and ionospheric convection has not been tested. Our aim is thus to test this understanding on a case study basis, which we do using quantitative measurements, and to discuss knowledge gaps.

We use upstream solar wind conditions (OMNI 1 min) to estimate Φ_D using the solar wind driving equation from *Milan et al.* [2012]. We obtain a time series of magnetospheric open flux content from auroral observations taken by the Imager for Magnetopause to Aurora Global Exploration (IMAGE) satellite. We combine these in a quantitative model relating Φ_D and F_{PC} to ionospheric flows, as shown in Figure 1. We then compare the model output with observations from DMSP ion drift meters, as indicated in red in Figure 1, and SuperDARN.

We present data from three separate days (2 October 2000, 4 November 2001, and 20 March 2005), where IMAGE and DMSP data were available. For the second day SuperDARN data were also available.

In section 2 we will discuss the data we use for our model comparison, specifics about the model [*Milan*, 2013] that we employ (section 2.1), and the results we find (section 2.4).

2. Data and Model Comparison

We employ the model of *Milan* [2013] to quantify ionospheric velocities based on the dayside and nightside reconnection. To run the model, we use OMNI- and IMAGE-derived data products and we then compare the model output velocities to ion drift meter data from the SSIES instrument [*Greenspan et al.*, 1986] on board the DMSP satellites and the SuperDARN data. In this section we first discuss the model and its data input and then the DMSP and SuperDARN data.

2.1. The Expanding and Contracting Polar Cap Model

The model we employ is equivalent to the one defined by *Milan* [2013], where a mathematical model of the expanding and contracting polar cap is used to quantify the strength of the flows in the ionosphere based on estimated dayside and nightside reconnection rates. In this section we describe the model, but a detailed mathematical description can be found in *Milan* [2013].

The model is very simple and as such, some assumptions and approximations are made. We assume an incompressible system, such that if $\Phi_D > \Phi_N$ the polar cap has to expand and if $\Phi_N > \Phi_D$, the polar cap has to decrease in size. Second, we assume a dipolar magnetic field, with the surface magnetic field strength at the equator being 31,000 nT. The model assumes that the polar cap, containing the open flux, F_{PC}, is circular, as is the equatorward boundary of the convection pattern. The OCB has a colatitude of λ_{OCB}, dictated by the amount of open flux. The colatitude of the equatorward boundary of the convection, the return flow boundary (RFB), is given by λ_{RFB}. As the polar cap expands and contracts under the action of Φ_D and Φ_N, the flows are determined based on the following assumptions: (a) the convective flows are incompressible, (b) nonreconnecting portions of the polar cap boundary are "adiaroic"; that is, the north-south component of the flow at the boundary is equal to the motion of the boundary itself [*Siscoe and Huang*, 1985], so that the electric field in the frame of reference moving with the boundary is zero.

Before we discuss our model-data comparison further (see section 2.4), we explain the origins of the data that we feed into the model.

2.2. Model Inputs

To run the model at any given time, six quantities are required: Φ_D, Φ_N, λ_{OCB}, λ_{RFB}, and the center coordinates (λ, θ) of the convection pattern, where λ is the geomagnetic colatitude and θ is the azimuth. The parameter θ is calculated with respect to local time with 0° being at 00 MLT.

The IMAGE satellite passed the auroral oval with a polar orbit (apogee at 44,000 km and perigee at 1000 km) and took complete images of the auroral oval at a cadence of ~2 min when the aurora was in view [*Mende et al.*, 2000a; *Burch*, 2000]. The Far Ultraviolet (FUV) instrument suite included two spectrographic imagers, SI12 and SI13 [*Burch*, 2000; *Mende et al.*, 2000b]. Here we use the SI12 data, which observed Lyman-α auroral emission (at 121.5667 nm this is primarily proton aurora) [*Mende et al.*, 2000b]. It was shown by

Sergeev et al. [1983] that the velocity distribution of the protons contributing to aurora must mean that they are on closed field lines. Further analysis by *Hubert et al.* [2006] and *Boakes et al.* [2008] show that the proton aurora can be used as an adequate locator of the OCB with the spatial uncertainty being small (~1°).

Concentric circles were fitted by eye to the poleward and equatorward edges of the auroral oval in IMAGE SI12 data as the locations of the OCB and RFB. From the OCB circles, F_{PC} was quantified assuming a dipolar magnetic field (a similar method to that employed by *Milan et al.* [2009]). Fitting circles or ovals to the inner boundary of the aurora gives very similar values for F_{PC}, but the locations of the flow boundaries will be slightly different. This is dealt with and explained in more detail further on (in section 3). The main reason why concentric circles were fitted to the data is the constraints of the model geometry, which requires circles as inputs.

Using auroral observations of the expanding/contracting auroral oval, *Milan et al.* [2012] found that the dayside reconnection rate, Φ_D, can be estimated as

$$\Phi_D = \Lambda V_X^{4/3} B_{YZ} \sin^{9/2} \frac{1}{2}\theta, \tag{2}$$

where Λ is a constant of proportionality ($= 3.3 \times 10^5$ m$^{2/3}$ s$^{1/3}$); V_X is the solar wind speed; B_{YZ} is the strength of the IMF, transverse to the flow direction; and θ is the clock angle of the IMF. We use data from the OMNI (1 min resolution) data set [*King and Papitashvili*, 2005] to calculate Φ_D. Using equation (1) with the time series for F_{PC} and Φ_D, we then also find Φ_N.

Milan et al. [2012] noted that, to bring the solar wind-estimated Φ_D to the same magnitudes as SuperDARN-derived Φ_{PC} values, 25 kV have to be added to Φ_D. *Milan* [2004, and references therein] calculated that residual flows may be of ~25 kV of the CPCP, setting the viscous interaction to orders of 10 kV. DMSP data analyzed by *Lockwood et al.* [2009] also suggested it may only be of the order of 10 kV. In this study, we thus add a constant 25 kV to Φ_D and Φ_N, to accommodate for any viscous-driven flows and possible underestimation of the reconnection rates.

The potentials calculated from the model are centered about the geomagnetic pole. We know from observations of the auroral oval, however, which we use as a locator of the polar cap, that its center is usually offset from the pole. Most notably, the center of the polar cap is shifted toward midnight by a few degrees (see, e.g., Figures 12 and 13 in *Shukhtina and Milan* [2014] or statistical study by *De La Beaujardière et al.* [1991]). We thus rotate the equations from *Milan* [2013], such that the center of the model output corresponds to the center of the fitted circles, rather than the pole.

The other necessary model inputs, θ_D and θ_N, the half sizes of the dayside and nightside merging gaps, are held at a constant 30° each, with respect to the center of the pattern (as was done by *Milan* [2013]). Figure 7 of *Milan* [2013] explores the possibility of a variable convection throat size. It shows that changing the merging gaps from being very narrow to very wide (θ_D and θ_N = 10° to 60°) has much less of an effect on the model output than changing the other variables, for example, the reconnection rates.

2.3. Comparative Data

We use ion drift meter data from the DMSP F12, F13, and F15 spacecraft [see *Heelis and Hanson*, 1998; *Hairston and Heelis*, 1996; *Rich and Hairston*, 1994, and references therein]. We only use the cross-track ion drift velocities, V_Y, as the along-track component is less reliable.

In our study we solely use data that were flagged as good by the data providers (see http://cindispace.utdallas.edu/DMSP/). We discard all DMSP orbits which have less than 100 good quality data points at geomagnetic latitudes above 50°. We then further discard any orbits that do not cross the areas encompassed by the return flow boundaries. It is well known that flows and aurora in the Northern and Southern Hemispheres are not always symmetrical [e.g., *Grocott et al.*, 2010; *Reistad et al.*, 2013]. All DMSP data obtained from the other hemisphere to the IMAGE data were thus discarded. For 2 October 2000 we have a total of 9 good DMSP polar crossings with overlapping IMAGE data, for 4 November 2001 we have 17 polar crossings, and for 20 March 2005 we have 13, giving us a total of 39 polar crossings for this study period.

We also use data from the Super Dual Auroral Radar Network (SuperDARN) [see *Milan et al.*, 2013; *Chisham et al.*, 2007, and references therein]. Ionospheric plasma inhomogeneities can scatter HF radar pulses back to the radars. The Doppler-shifted signals are then used to determine the line-of-sight ionospheric flow velocities. Coverage of a large proportion of the polar ionosphere in the Northern Hemisphere then allows

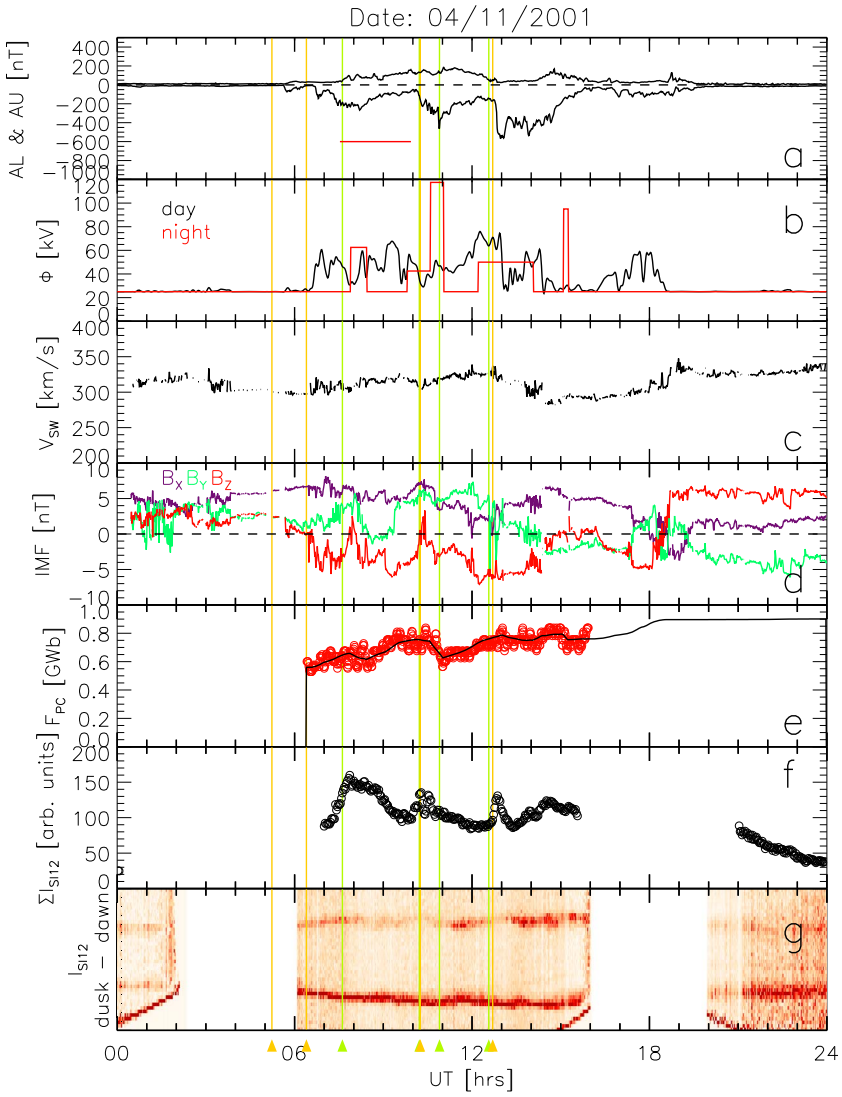

Figure 2. Data for the interval of interest (4 November 2001). The panels show (a) *AL* and *AU*; (b) $\Phi_D + 25$ kV (black) and $\Phi_N + 25$ kV (red); (c) V_{SW}; (d) IMF B_X (purple), B_Y (green), and B_Z (red); (e) F_{PC} (data in red and estimator used to calculate Φ_N in black); (f) total auroral brightness (from SI12 instrument) in arbitrary units; (g) dusk-dawn keogram of the proton aurora (from SI12 instrument), reaching down to 40° of colatitude. The green/orange arrows (top and bottom) and green/orange lines indicate substorm onsets, from Frey's and the SuperMAG event lists, respectively.

fitting the data to models (parameterized by the solar wind) of global convection using spherical harmonic fitting (see *Ruohoniemi and Baker* [1998] for method). From the global convection pattern it is then possible to extract flow velocities even in places where there are no direct measurements. This provides us with another data set to compare the model to.

To compare the DMSP convection measurements with the model, we resolve the model output into the cross-track direction. We do the same with the SuperDARN flows so we can compare with DMSP and the model.

2.4. Results

Figure 2 gives an overview of 4 November 2001. Figures 2c and 2d show the solar wind conditions for this day with the IMF conditions and the solar wind speed. The solar wind speed was almost constant, at 320 km/s, throughout the day. Before 06 UT and after 18 UT the IMF B_Z was directed northward. In the intervening period, the IMF B_Z was southward with $B_Z \sim -5$ nT.

Figure 2a shows a summary of the magnetospheric response to these solar wind conditions, with the auroral upper and lower electrojet indices, *AL* and *AU*, for this day. *AU* and *AL* were very quiet for the periods of northward IMF. AL bays suggest substorm onsets near 07 UT, 10 UT, and 12:45 UT. The red line in this panel shows a steady magnetospheric convection event (SMC), identified by *Walach and Milan* [2015]. This SMC followed a substorm; see *Walach and Milan* [2015] and references therein, for detailed information of the convection dynamics about this event type.

Figure 2g shows a dusk-dawn slice, or auroral keogram, of the SI12 data, evolving with time. Each slice's center shows the geomagnetic pole, stretching toward 40° of geomagnetic colatitude toward dusk (bottom) and dawn (top). The keogram shows the auroral brightness with light and dark red indicating the least bright and brightest pixels, and white showing data gaps. From Figures 2g and 2e we see how the auroral oval expands equatorward (the top and bottom of the panel) before substorm onsets and with a subsequent contraction as the substorms progress.

Figure 2f shows the total auroral brightness calculated from SI12 (see *Shukhtina and Milan* [2014], for measuring technique) (in arbitrary units). Peaks in brightness are seen at the time of substorm onset.

The red circles in Figure 2e show F_{PC} measurements based on the circles fitted to the inner auroral boundary. These were smoothed over three data points to reduce quantization noise.

Φ_N was obtained by fitting calculated values of F_{PC} to the slope of F_{PC}, using $\frac{dF_{PC}}{dt} = \Phi_D - \Phi_N$. Initially, Φ_N was kept at 0 kV and then incrementally changed, such that the curve of calculated F_{PC} matched the measured F_{PC} as closely as possible (a similar technique was used by *Milan et al.* [2007]). The black line shows the final curve of F_{PC}, which was used to calculate Φ_N, and the red shows the F_{PC} measurements. Figure 2b shows Φ_D and Φ_N with the extra 25 kV added on.

Substorm onsets, as identified by *Frey et al.* [2004] from the IMAGE data set, are indicated by the green triangles below Figure 2g and the vertical green lines, whereas the orange triangles and vertical lines show substorms identified by the SuperMAG data set [*Newell and Gjerloev*, 2011]. All the Frey substorm onsets, except for the second one, appear to be well identified, as they match auroral brightenings and expansions. Leading up to a substorm we would expect the aurora to expand equatorward and thus F_{PC} increases (Figure 2e). At onset the nightside aurora brightens explosively (Figure 2f) and contracts again (as shown in Figures 2e and 2g) (these features are further discussed in *Walach and Milan* [2015]). There are some discrepancies between the substorm timings and the onset timings of SuperMAG substorms. For the first two SuperMAG substorms there are not enough auroral data to discuss them in detail, but the third and last one occur within minutes of a Frey substorm, giving us confidence in the timing of the onset.

The IMF conditions for this day are not excessively active, but there is dayside driving of the magnetosphere, as Φ_D is elevated. The B_Y component of the IMF is ~4–7 nT from 9:30 UT until 12:30 UT, but is otherwise between −2 and 2 nT.

Figures 3 and 4 all show individual polar passes of DMSP F12, F13, and F15, which were used in this study. Each orbit shows the IMAGE SI12 FUV data in a white to red map in the top left panel (the same color scheme as the keogram in Figure 2). The dark red circles indicate the concentric boundaries used for the model. Each DMSP pass shows the cross-track velocity measurements in black lines (grey for quality flags other than "good") (bottom left panel). The black potential patterns in the top right panels are derived from the model with the cross-track velocity component shown in blue along the DMSP trajectory. Green contours (bottom left panel where applicable) show the SuperDARN convection equipotentials. The dotted grey circles indicate concentric circles spaced at 10° around the geomagnetic pole. Each panel has the hemisphere of the DMSP pass indicated to the left, followed by which satellite the measurements were obtained from and the time at which the satellite was closest to the pole (i.e., time at the center of the polar pass). The number to the right side of the polar pass panels with SuperDARN data indicates the number of SuperDARN measurements where the green potential pattern was based on, with 100 being the minimum requirement.

The potential patterns obtained by the model for 4 November 2001 (see Figure 3 are rotated by 1 h MLT in a westerly direction. This was done to accommodate the persistent rotation in the convection throat seen in the SuperDARN patterns throughout this day. If we were to use cross-track DMSP data alone, we would not be able to pick up any such asymmetries in the convection patterns. Similarly, *Ruohoniemi and Greenwald* [2005] find also that statistically, the convection pattern appears rotated in a westerly direction during southward IMF B_Z. The mechanisms and time scales on which these pattern shifts occur are however

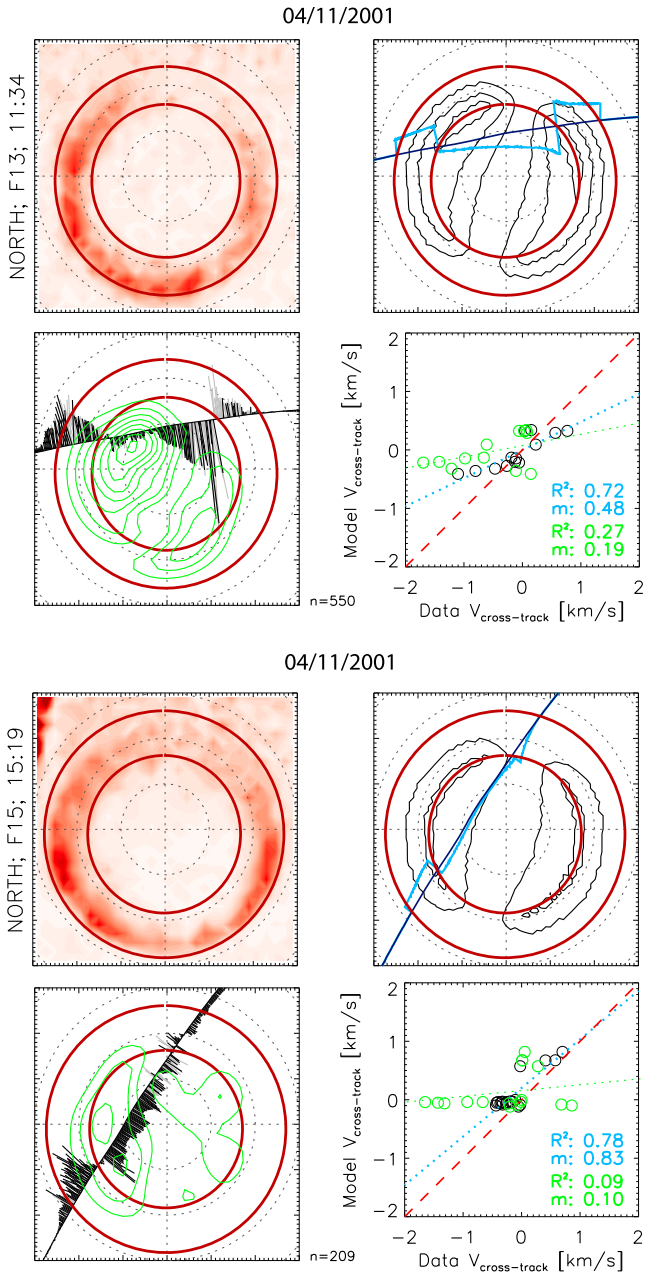

Figure 3. Two individual DMSP orbits for 4 November 2001, showing the IMAGE data with (top left) fitted circles (colored map); (top right) the model equipotentials (black) and cross-track velocities (blue); (bottom right) DMSP cross-track velocities and SuperDARN equipotentials and a scatterplot of the cross-track velocities. The potentials are spaced at regular intervals of 6 kV. Each orbit is centered on the geomagnetic poles, and the concentric circles in dashed grey are spaced at 10° of geomagnetic latitudes each. The green data in the scatterplots show the cross-track velocities derived from SuperDARN. The red dashed line shows the line of unity, and the dotted lines show the lines of best fit (green = SuperDARN and blue = DMSP).

not well enough understood yet [see, e.g., *Grocott et al.*, 2008] to incorporate them into the model, so we have made a first rudimentary effort to accommodate for it. In some locations, especially near the merging gaps in the first pass shown in Figure 3, we see additional rotations in the pattern, associated with IMF B_Y, which are not reproduced by the model. As a result of the rotation of the convection pattern, the "centers" of the modeled equipotentials are generally more accurately aligned with the ones computed by SuperDARN than they were before. As the SuperDARN coverage for the 2 October 2000 and the 20 March 2005 are not very good,

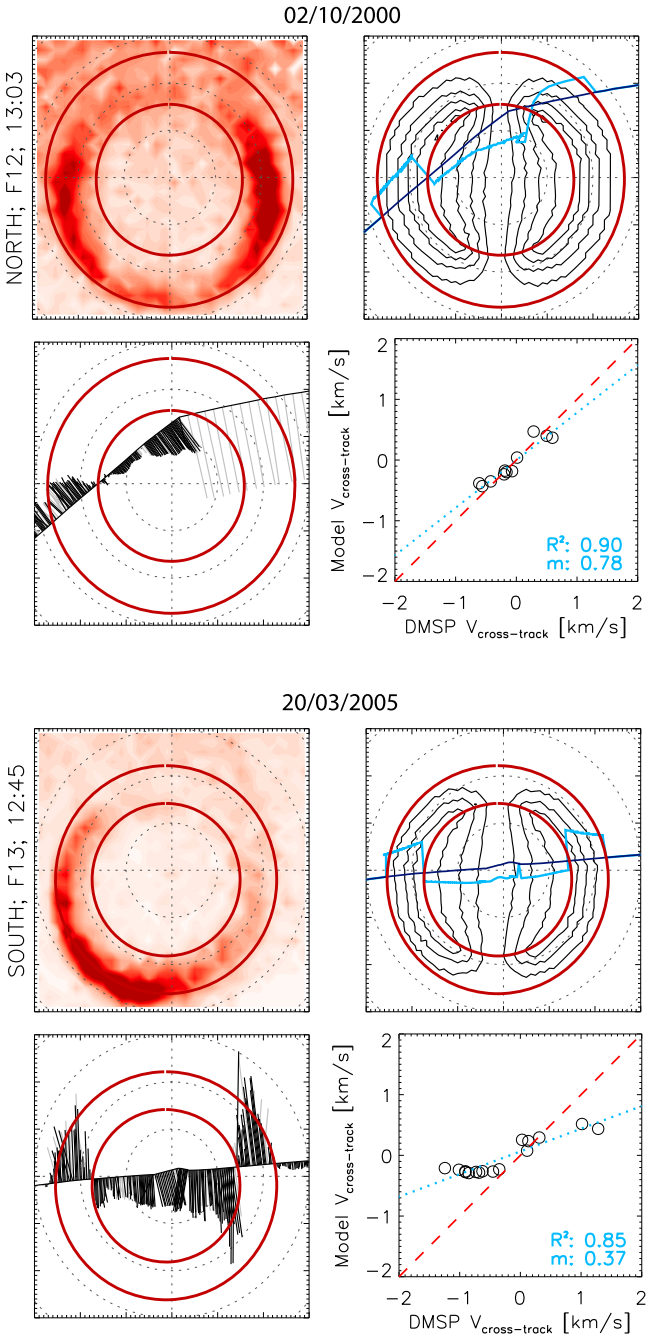

Figure 4. Two individual DMSP orbits for 2 October 2000 and 20 March 2005, presented in the same way as the data in Figure 3.

we have not included these data here and chosen not to make any guesses about dawn-dusk asymmetries in the convection pattern.

Overall, a visual inspection of the maps in Figures 3 and 4 suggests that the locations, directions, and magnitudes of the flow velocities are estimated well, but problems arise near the boundaries: DMSP measures flows which gradually change from one extreme to the other across a boundary, whereas the model's flow regimes change more abruptly. We postulate that this is due to the distributed nature of the field-aligned currents, as the model presumes that these boundary regions are infinitely thin. The result is that the largest flow velocities are underestimated, the medium scale flows are estimated well and the very slow speeds near the

boundaries are overestimated by the model. This effect can clearly be seen in the first orbit in Figure 3 in the return flow regions.

The bottom right panels for Figures 3 and 4 show the data of the polar passes in a different format. Here we show scatterplots of the cross-track model velocities versus the cross-track DMSP velocities (black points) and the model-derived cross-track velocities against the SuperDARN-derived cross-track velocities (green points). To reduce some of the most obvious problems with the data, namely, changes in the convection pattern that occur on smaller time scales than the time taken by DMSP to pass the flow regions (~10–15 min) and the regions near the boundaries being misrepresented by the model, the data were processed slightly from the polar pass panels to the scatter panels. For this the DMSP data were first split into intervals where IMAGE data were available (usually ~2 min length). For each of these data bins the model input was adjusted to represent the changes in the polar cap and reconnection rates. We then discard any data within $\pm 1^\circ$ of any boundary and average over 10 data points. Binning the data and varying the model input achieves that the outcome is less affected by quickly varying reconnection rates. Only considering data which are not in the vicinity of the boundaries and taking averages over 10 data points accomplishes that the abrupt changes in the model velocities, which are not always physical, have less weighting in the analysis. These processed data are used for the scatterplots.

The dotted lines in the scatterplots indicate the line of best fit, calculated using linear regression, whereas the red dashed line shows the line of unity. The general trend that we already saw in the pass plots, with the model underestimating both the DMSP data and the SuperDARN-derived velocities is mirrored here. If the model estimated all flows well, the correlation coefficient, R^2, and the gradient, m, would both always be equal to 1.

The first pass projection in Figure 3 does not show a very good match between the model and the SuperDARN velocities, but the DMSP velocities agree well with the model (R^2 of 0.72).

The second orbit in Figure 3 is yet another example, where the SuperDARN data do not match the model very well. This is perhaps partially due to fewer SuperDARN data points being available, so the data are less reliable. The SuperDARN flows are underestimated, resulting in the distinct horizontal scatter of the points in the plot.

Both satellite passes in Figure 3 show examples where the model velocities match the DMSP measurements better than the SuperDARN velocities. This is because both the model and DMSP show fairly large flows in the morning sector of the flow regions, whereas SuperDARN sees no flows there and instead larger flows in the dusk cell.

The first pass in Figure 4 shows the highest correlation ($R^2 = 0.90$) for the model versus the DMSP measurements, even though only two thirds of the DMSP data were usable. The gradient of the linear regression is also quite close to 1 at 0.78.

An example where the boundary evaluations are poor is given by the second orbit in Figure 4. The correlation in the scatterplot shows a good agreement between model and data ($R^2 = 0.85$), but the velocities are underestimated, which is likely due to an underestimation of the reconnection rates. This becomes apparent when looking at the pass plot or the gradient in the scatterplot ($m = 0.37$).

Figure 5 shows a summary of all the polar passes of DMSP from the three time periods. The data shown here were obtained in the same way as the data shown in the individual scatterplots, but all orbits for each day were combined in one panel. The different colors correspond to each of the three days: green crosses show data from 2 October 2000, black circles show data from 4 November 2001, and orange diamonds show data from 20 March 2005. The corresponding R^2 and m are shown in the same colors, along with the line of best fit. The R^2 and m values in purple show the linear regression for the entire data set (i.e., all three days combined).

Overall, the modeled flows are broadly consistent with the data, but they are often underestimated, as already shown. Indeed m indicates that the model flows are approximately a third of the magnitude of the DMSP measurements, but R^2 and the overall data distribution indicate a correlation of the model and the data, showing that the model nowcasts the trends in the flows well. The results from the three days considered were broadly consistent with each other and the scatter of the points was very similar too.

3. Discussion

The expanding and contracting polar cap model has been used for decades to discuss and explain ionospheric and magnetospheric convection flows, but it has never been tested qualitatively in terms of ionospheric flows.

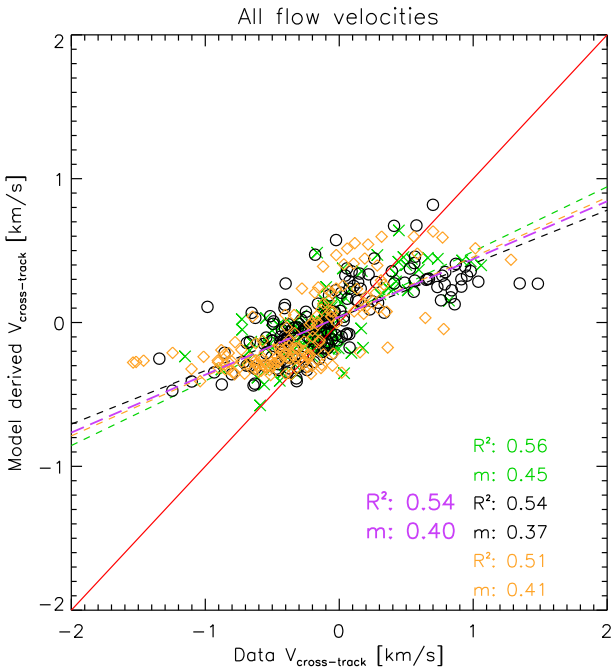

Figure 5. Scatterplot of cross-track velocities derived from the model against all the cross-track velocities measured by DMSP for each polar pass of the three selected time periods. The green crosses show the data for 2 October 2000, the black circles show data for 4 November 2001 and the orange diamonds show data for 20 March 2005. The colored dashed lines R^2 and m values show the lines of best fit for each day, with the colors corresponding to the symbol colors. The red line shows the line of unity and the long dashed purple line shows the line of best fit for the entire data set. The corresponding values (R^2 and m) are also shown in purple.

3.1. The ECPC Model

Other models for the ECPC are discussed quantitatively, for example, by *Lockwood* [1991], who explored the necessity of allowing the expanding and contracting polar cap model to hold a history of previous polar cap flows. Although the model we employ has no memory per se, the history of the system is kept in the time series of F_{PC}. A very similar model based on the ECPC has also been developed by *Lockwood and Morley* [2004], involving, however, a time-delayed magnetospheric reaction, which we do not have here. Their model is more sophisticated and as such, requires further information for the model input, for example, the speed of the flows across the merging gap. Another model based on the ECPC was formulated by *Freeman* [2003], but their model does not include the nightside reconnection rate. In this study we use a simple model of the expanding and contracting polar cap [*Milan*, 2013] to calculate ionospheric velocities using changes in Φ_D, Φ_N, and the flow regions, assuming an incompressible ionosphere and circular symmetry. We compare the model flow velocities to in situ measurements from the ion drift meter on board the DMSP satellites and ground-based measurements from SuperDARN. This study outlines some distinct weaknesses of the model which we will now discuss in more detail. While the simplicity allows the model to be driven by our understanding of the physical processes, it also imposes some constraints on our study.

3.2. Model Inputs

Two input values (θ_D and θ_N, the widths of the merging gaps), were picked to be fixed constants that the authors thought to be appropriate from visual inspection of the data. *Milan* [2013] showed that varying these values does not have a significant impact on the polar cap dynamics [see *Milan*, 2013, Figure 7]. It is however possible that these values may vary with time. For example, they may be dependent on solar wind driving of the magnetosphere or activity within the magnetosphere-ionosphere system. If this is the case, we think it would lead to the largest discrepancies, during more active periods. For example, *Milan et al.* [2016] showed that during flux transfer events when the solar wind was traveling at larger speeds, θ_D must have spanned more hours of MLT than otherwise (results show that $V_{SW} = 380$ km/s lead to $\theta_D = 30°$ and $V_{SW} = 650$ km/s lead to a merging line width of up to 105°). As V_{SW} is very constant and not excessively high during the period of interest here, we assume the 30° is a fair estimate.

Increasing Φ_D and Φ_N, has the clear result that the magnitudes of the modeled velocities and electrostatic potential increase. Changing the sizes and locations of the open closed field line boundary and the return flow boundary would change the patterns of the flows.

3.3. Irregular and Time-Dependent Flows

The first orbit in Figure 4 shows an example of an orbit where considerable convection occurs outside the polar cap and auroral zones. An example of irregular sunward flows which can occur on latitudes much lower than the auroral oval are subauroral polarization streams (SAPs) [see, e.g., *Foster and Vo*, 2002, and references therein]. SAPs occur mainly on the duskside in the Northern Hemisphere and appear separated latitudinally from the dual-cell convection pattern with possible peak velocities above 1 km/s, which the model does not allow for. The flows we see outside the auroral oval, however, appear as part of the dual-cell convection pattern, so they may not be SAPs.

A further problem presents itself in that the magnetosphere dynamics change on short time scales, for example, during substorm onset and the early stages of substorm expansion [see, e.g., *Akasofu*, 1964], but the DMSP spacecraft take much longer to traverse one polar cap (up to ~27 min). As the polar cap dynamics and flows can change on a time scale of minutes, any orbital plots close to substorm onset will show some flows from just before and during the substorm but perhaps even from the recovery phase. [*Lockwood and Freeman*, 1989]. We tried to overcome this by varying the model input for the scatterplots, which appears to improve the model-data fits.

As previously discussed by *Morley and Lockwood* [2006], the time scales on which magnetospheric flows respond to reconnection and especially how the polar cap expands in shape may be variable. As such, the assumption of the polar cap expanding and contracting at the first instance radially, as opposed to just at the merging gaps with a time delay on the whole convection pattern, has been discussed and modeled in different ways. A comparison of such models was also discussed in depth by *Freeman* [2003], leading to the conclusion that the overall modeled velocities are very similar. Modeling the convection pattern with an instantaneous response will most likely introduce the largest errors when there is a sudden change in the solar wind driving (for example, if the IMF is pointing northward for a prolonged period of time and then observes a sudden southward turning). As such, it may be a source of error, especially when the reconnection rates change.

Furthermore, the assumption of the electric potential pattern being static, but instantly responsive, has also been challenged in the past, as discussed by *Morley and Lockwood* [2006] and references therein. However, we conclude that the assumption of a static pattern is fair due to the time resolution of our data (i.e. minutes).

3.4. SuperDARN Data Comparison

Figure 2 shows an enhanced and steady IMF B_Y component for many hours before the shown orbits (Figure 3), which results in an imbalance in the size of the dawn and dusk ionospheric convection cells and a dawnward rotation of the dayside merging line [*Cowley et al.*, 1991; *Ruohoniemi and Greenwald*, 1996]. This trend persists throughout most of the interval shown for this day. When we compare the convection patterns to the SuperDARN patterns, we also see small scale features, such as crinkled flows across the polar cap or a further rotation at the Harang discontinuity [*Harang*, 1946; *Heppner*, 1972] in the SuperDARN data that the model can obviously not infer. To make future models more physically accurate, asymmetries arising in the Northern and Southern Hemispheres and IMF B_Y-induced asymmetries will have to be addressed.

Despite the northern polar region being well covered by SuperDARN observations, there are still many instances where even when many data points are available ($n \geq 200$), they seldom fall in the same place as DMSP observations. As such, the SuperDARN data we use for the direct one-to-one comparison in Figure 3 are deduced from the overall SuperDARN convection pattern, imposing a trade-off of quality versus quantity of observations [*Ruohoniemi and Baker*, 1998]. Furthermore, as there are sometimes spatial data gaps in the SuperDARN coverage across the dayside, there tends to be a shift of the convection pattern on the dayside toward the pole due to a lack of data being filled in by the empirical models [*Ruohoniemi and Greenwald*, 1996].

3.5. Underestimation of Flows

We tried to overcome the possible underestimation of reconnection rates or viscous interaction (the implications on the CPCP would be the same) by adding 25 kV to both Φ_D and Φ_N. The size of the viscous interaction, and how it may change with differing solar wind conditions, is however still poorly understood [*Milan*, 2004].

Even though we added 25 kV to Φ_D and Φ_N, the model underestimates the flows measured by DMSP (see Figures 3–5). The scatterplots shown suggest that the DMSP data are underestimated by a factor

of 2–3. A similar offset in flow magnitudes was found statistically between SuperDARN and DMSP data by *Xu et al.* [2008] and *Drayton et al.* [2005], with SuperDARN velocities being ~30% smaller than DMSP velocities. Furthermore, *Xu et al.* [2001], *Gillies et al.* [2011], and *Davies et al.* [1999] all used different methods to show that SuperDARN tends to underestimate flows, indicating that the model must also be underestimating the flows, despite the additional 25 kV added to the dayside and nightside reconnection rates. Studies by *Gillies et al.* [2009, 2010, 2011, 2012] showed that the methods employed to obtain ionospheric convection velocities from SuperDARN data tend to not consider the refractive index of the ionosphere. This is due to the refractive index being obtained using a large volume of the ionosphere and nonlocalized electron densities, rather than more refined measurements. The studies by *Drayton et al.* [2005] and *Gillies et al.* [2009, 2012] only used line-of-sight SuperDARN data, which may add a geometrical error to comparing the SuperDARN and DMSP data sets. As was shown by *Imber* [2008], when SuperDARN data from the same location in the cross-track direction are compared to DMSP data statistically, the two data sets do match very well (this will also be explored in a future study). The SuperDARN data which we show in our model-data comparison were obtained from SuperDARN potential maps, as even though good coverage was available for one of the days studied, the SuperDARN measurements did not coincide spatially with the location of the DMSP pass.

Above all, our analysis shows that flow velocities from DMSP can be nowcasted qualitatively when the convection is driven by dayside and nightside reconnection (i.e., when a dual-cell convection pattern is dominant).

4. Concluding Remarks

This study has investigated the convection velocities, calculated with the simple expanding-contracting polar cap model. The quantitative analysis show that the magnitudes of the flows are, on average, underestimated by a factor of 2–3 but can be estimated qualitatively. We conclude that the offsets may well be a combination of both measurement errors and underestimation of reconnection rates, but the simplicity of the model adds to the effect that flows are underestimated. Overall, the locations of the flows match the auroral boundaries well and the relative flow magnitudes agree well.

The main weakness of the considered model itself is that the convection cells, and indeed the polar cap itself, are not always symmetric. In order to improve the model's prediction capabilities, as well as to bring our understanding forward, more research into the angular width of the merging lines and the IMF B_Y-induced asymmetries is required. Although the auroral boundaries represent the flow boundaries very well, the model predicts sharp edges as the boundaries are assumed to be infinitely thin sheets, which is not representative of the data.

We conclude that although we can predict the flow strengths, B_Y-related asymmetries must be built into the model in order to predict flows more accurately, as a simple rotation of the convection pattern is not enough to compensate for asymmetries.

Acknowledgments
We thank the PI of IMAGE, J.L. Burch and the PI of FUV, S.B. Mende for the original IMAGE data set. The OMNI data are provided by the GSFC/SPDF OMNIWeb platform (http://cdaweb.gsfc.nasa.gov/), and we are grateful to the PIs of the data set used: J.H. King and N. Papatashvilli. We gratefully acknowledge the Center for Space Sciences at the University of Texas at Dallas and the U.S. Air Force for providing the DMSP ion drift meter data. We thank H. Frey for the IMAGE-derived substorm event list and the SuperMAG team for providing their substorm event list on their website (http://supermag.uib.no/substorms/). M.-T.W. was supported by a studentship from the Science and Technology Facilities Council, UK. S.E.M. and T.K.Y. were supported on the STFC grant ST/K001000/1. The SuperDARN data processing was supported by the European Union Framework 7 Programme, ECLAT Project grant 263325 and the data are available on the cluster science archive (http://www.cosmos.esa.int/web/csa). T.K.Y. was also supported on the NERC grant NE/K011766/1. The original IMAGE data are available through the IMAGE FUV homepage (http://sprg.ssl.berkeley.edu/image/) and the DMSP data are available via the DMSP SSIES website (http://cssxp1000.utdallas.edu/DMSP/dmsp_data_at_utdallas.html). The code used to generate the plots in this paper are stored in the University of Leicester computers and are available on request.

References

Akasofu, S.-I. (1964), The development of the auroral substorm, *Planet. Space Sci.*, *12*, 273–282.
Boakes, P. D., S. E. Milan, G. A. Abel, M. P. Freeman, G. Chisham, B. Hubert, and T. Sotirelis (2008), On the use of IMAGE FUV for estimating the latitude of the open/closed magnetic field line boundary in the ionosphere, *Ann. Geophys.*, *26*, 2759–2769, doi:10.5194/angeo-26-2759-2008.
Burch, J. L. (2000), IMAGE mission overview, *Space Sci. Rev.*, *91*, 1–14.
Chisham, G., et al. (2007), A decade of the Super Dual Auroral Radar Network (SuperDARN): Scientific achievements, new techniques and future directions, *Surv. Geophys.*, *28*(1), 33–109, doi:10.1007/s10712-007-9017-8.
Cowley, S. W. H., and M. Lockwood (1992), Excitation and decay of solar wind-driven flows in the magnetosphere-ionophere system, *Ann. Geophys.*, *10*, 103–115.
Cowley, S. W. H., and M. Lockwood (1996), Time-dependent flows in the coupled solar wind-magnetosphere-ionosphere system, *Adv. Space Res.*, *18*(8), 141–150, doi:10.1016/0273-1177(95)00972-8.
Cowley, S. W. H., J. P. Morelli, and M. Lockwood (1991), Dependence of convective flows and particle precipitation in the high-latitude dayside ionosphere on the *X* and *Y* components of the interplanetary magnetic field, *J. Geophys. Res.*, *96*(A4), 5557–5564.
Davies, J. A., M. Lester, S. E. Milan, and T. K. Yeoman (1999), A comparison of velocity measurements from the CUTLASS Finland radar and the EISCAT UHF system, *Ann. Geophys.*, *17*(7), 892–902, doi:10.5194/angeo-17-892-1999.
De La Beaujardière, O., D. Alcayde, J. Fontanari, and C. Leger (1991), Seasonal dependence of high-latitude electric fields, *J. Geophys. Res.*, *96*(A4), 5723–5735.
Drayton, R. A., A. V. Koustov, M. R. Hairston, and J.-P. Villain (2005), Comparison of DMSP cross-track ion drifts and SuperDARN line-of-sight velocities, *Ann. Geophys.*, *23*, 2479–2486.
Dungey, J. W. (1963), Interactions of solar plasma with the geomagnetic field, *Planet. Space Sci.*, *10*, 223–237.
Foster, J. C. (1983), An empirical electric field model derived from Chatanika radar data, *J. Geophys. Res.*, *88*(A2), 981–987.

Foster, J. C., and H. B. Vo (2002), Average characteristics and activity dependence of the subauroral polarization stream, *J. Geophys. Res.*, *107*(A12), 1475, doi:10.1029/2002JA009409.
Freeman, M. P. (2003), A unified model of the response of ionospheric convection to changes in the interplanetary magnetic field, *J. Geophys. Res.*, *108*(A1), 1024, doi:10.1029/2002JA009385.
Freeman, M. P., and D. J. Southwood (1988), The effect of magnetospheric erosion on mid- and high-latitude ionospheric flows, *Planet. Space Sci.*, *36*(5), 509–522, doi:10.1016/0032-0633(88)90110-9.
Frey, H. U., S. B. Mende, V. Angelopoulos, and E. F. Donovan (2004), Substorm onset observations by IMAGE-FUV, *J. Geophys. Res.*, *109*, A10304, doi:10.1029/2004JA010607.
Gillies, R. G., G. C. Hussey, G. J. Sofko, K. A. McWilliams, R. A. D. Fiori, P. Ponomarenko, and J. P. St.-Maurice (2009), Improvement of SuperDARN velocity measurements by estimating the index of refraction in the scattering region using interferometry, *J. Geophys. Res.*, *114*, A07305, doi:10.1029/2008JA013967.
Gillies, R. G., G. C. Hussey, G. J. Sofko, D. M. Wright, and J. A. Davies (2010), A comparison of EISCAT and SuperDARN *F*-region measurements with consideration of the refractive index in the scattering volume, *J. Geophys. Res.*, *115*, A06319, doi:10.1029/2009JA014694.
Gillies, R. G., G. C. Hussey, G. J. Sofko, P. V. Ponomarenko, and K. A. McWilliams (2011), Improvement of HF coherent radar line-of-sight velocities by estimating the refractive index in the scattering volume using radar frequency shifting, *J. Geophys. Res.*, *116*, A01302, doi:10.1029/2010JA016043.
Gillies, R. G., G. C. Hussey, G. J. Sofko, and K. A. McWilliams (2012), A statistical analysis of SuperDARN scattering volume electron densities and velocity corrections using a radar frequency shifting technique, *J. Geophys. Res.*, *117*, A08320, doi:10.1029/2012JA017866.
Greenspan, M. E., P. B. Anderson, and J. M. Pelagatti, (1986), Characteristics of the Thermal Plasma Monitor (SSIES) for the Defense Meteorological Satellite Program (DMSP), Spacecraft S8 through S10, *Tech. Rep.*, Regis College Research Center, Weston, Mass.
Grocott, A., S. Cowley, J. Sigwarth, J. Watermann, and T. K. Yeoman (2002), Excitation of twin-vortex flow in the nightside high-latitude ionosphere during an isolated substorm, *Ann. Geophys.*, *20*, 1577–1601, doi:10.5194/angeo-20-1577-2002.
Grocott, A., S. W. H. Cowley, and J. B. Sigwarth (2003), Ionospheric flow during extended intervals of northward but B_y-dominated IMF, *Ann. Geophys.*, *21*(2), 509–538, doi:10.5194/angeo-21-509-2003.
Grocott, A., S. E. Milan, and T. K. Yeoman (2008), Interplanetary magnetic field control of fast azimuthal flows in the nightside high-latitude ionosphere, *Geophys. Res. Lett.*, *35*, L08102, doi:10.1029/2008GL033545.
Grocott, A., S. E. Milan, T. K. Yeoman, N. Sato, A. S. Yukimatu, and J. A. Wild (2010), Superposed epoch analysis of the ionospheric convection evolution during substorms: IMF B_y dependence, *J. Geophys. Res.*, *115*, A00I06, doi:10.1029/2010JA015728.
Hairston, M. R., and R. A. Heelis, (1996), Analysis of ionospheric parameters based on DMSP SSIES data using the DBASE4 and NADIA programs, *Tech. Rep.*, Phillips Laboratory, Directorate of Geophysics, Hanscom Air Force Base, Massachusetts.
Harang, L. (1946), The mean field of disturbance of polar geomagnetic storms, *Terr. Magn. Atmos. Electric.*, *51*(3), 353–380, doi:10.1029/TE051i003p00353.
Heelis, R. A., and W. B. Hanson (1998), Measurements of thermal ion drift velocity and temperature using planar sensors, in *Measurement Techniques in Space Plasmas: Particles, Geophys. Monogr. Ser.*, vol. 102, p. 61, AGU, Washington, D. C.
Heppner, J. P. (1972), The harang discontinuity in auroral belt ionospheric currents, in *A Collection of Articles on Cosmic Geophysics Dedicated to the Memory of Professor L. Harang on the Seventieth Anniversary of His Birth 19 April 1972*, 29 edn., edited by J. Holtet and A. Egeland, pp. 105–120, Geofysiske Publikasjoner; Universitetsforlage, Oslo.
Heppner, J. P. (1977), Empirical models of high-latitude electric fields, *J. Geophys. Res.*, *82*(7), 1115–1125.
Heppner, J. P., and N. C. Maynard (1987), Empirical high-latitude electric field models, *J. Geophys. Res.*, *92*(A5), 4467–4489, doi:10.1029/JA092iA05p04467.
Hubert, B., S. E. Milan, A. Grocott, C. Blockx, S. W. H. Cowley, and J.-C. Gérard (2006), Dayside and nightside reconnection rates inferred from IMAGE FUV and Super Dual Auroral Radar Network data, *J. Geophys. Res.*, *111*, A03217, doi:10.1029/2005JA011140.
Imber, S. M. (2008), Auroral and ionospheric flow measurements of magnetopause reconnection during intervals of northward interplanetary magnetic field, PhD thesis, Univ. of Leicester, Leicester, U. K.
King, J. H., and N. E. Papitashvili (2005), Solar wind spatial scales in and comparisons of hourly Wind and ACE plasma and magnetic field data, *J. Geophys. Res.*, *110*, A02104, doi:10.1029/2004JA010649.
Lockwood, M. (1991), On flow reversal boundaries and transpolar voltage in average models of high-latitude convection, *Planet. Space Sci.*, *39*(3), 397–409, doi:10.1016/0032-0633(91)90002-r.
Lockwood, M., and S. W. H. Cowley (1992), Ionospheric convection and the substorm cycle, in *International Conference on Substorms*, pp. 99–109, Eur. Space Agency Publ., Noordwijk, Netherlands.
Lockwood, M., and M. P. Freeman (1989), Recent ionospheric observations relating to solar-wind-magnetosphere coupling, *Philos. Trans. R. Soc.*, *328*, 93–105.
Lockwood, M., and S. K. Morley (2004), A numerical model of the ionospheric signatures of time-varying magnetic reconnection: I. Ionospheric convection, *Ann. Geophys.*, *22*, 73–91.
Lockwood, M., M. Hairston, I. Finch, and A. Rouillard (2009), Transpolar voltage and polar cap flux during the substorm cycle and steady convection events, *J. Geophys. Res.*, *114*, A01210, doi:10.1029/2008JA013697.
Mende, S. B., et al. (2000a), Far ultraviolet imaging from the IMAGE spacecraft. 2. Wideband FUV imaging, *Space Sci. Rev.*, *91*, 271–285.
Mende, S. B., et al. (2000b), Far ultraviolet imaging from the IMAGE spacecraft. 3. Spectral imaging of Lyman-α and OI 135.6 nm, in *The IMAGE Mission*, edited by J. L. Burch, chap. 3, pp. 287–318, Springer, Netherlands.
Milan, S. E. (2004), Dayside and nightside contributions to the cross polar cap potential: Placing an upper limit on a viscous-like interaction, *Ann. Geophys.*, *22*, 3771–3777, doi:10.5194/angeo-22-3771-2004.
Milan, S. E. (2013), Modeling Birkeland currents in the expanding/contracting polar cap paradigm, *J. Geophys. Res. Space Physics*, *118*, 5532–5542, doi:10.1002/jgra.50393.
Milan, S. E., G. Provan, and B. Hubert (2007), Magnetic flux transport in the Dungey cycle: A survey of dayside and nightside reconnection rates, *J. Geophys. Res.*, *112*, A01209, doi:10.1029/2006JA011642.
Milan, S. E., J. Hutchinson, P. D. Boakes, and B. Hubert (2009), Influences on the radius of the auroral oval, *Ann. Geophys.*, *27*, 2913–2924.
Milan, S. E., J. S. Gosling, and B. Hubert (2012), Relationship between interplanetary parameters and the magnetopause reconnection rate quantified from observations of the expanding polar cap, *J. Geophys. Res.*, *117*, A03226, doi:10.1029/2011JA017082.
Milan, S. E., S. Imber, and M. Lester, (2013), ECLAT SuperDARN user guide, *Tech. Rep.*, Univ. of Leicester, Leicester, U. K.
Milan, S. E., S. M. Imber, J. A. Carter, M.-T. Walach, and B. Hubert (2016), What controls the local time extent of flux transfer events?, *J. Geophys. Res. Space Physics*, *121*, 1391–1401, doi:10.1002/2015JA022012.

Morley, S. K., and M. Lockwood (2006), A numerical model of the ionospheric signatures of time-varying magnetic reconnection: III. Quasi-instantaneous convection responses in the Cowley-Lockwood paradigm, *Ann. Geophys.*, *24*, 961–972, doi:10.5194/angeo-24-961-2006.

Newell, P. T., and J. W. Gjerloev (2011), Evaluation of SuperMAG auroral electrojet indices as indicators of substorms and auroral power, *J. Geophys. Res.*, *116*, A1211, doi:10.1029/2011JA016779.

Reistad, J. P., N. Østgaard, K. M. Laundal, and K. Oksavik (2013), On the non-conjugacy of nightside aurora and their generator mechanisms, *J. Geophys. Res. Space Physics*, *118*, 3394–3406, doi:10.1002/jgra.50300.

Rich, F. J., and M. Hairston (1994), Large-scale convection patterns observed by DMSP, *J. Geophys. Res.*, *99*(A3), 3827–3844.

Ruohoniemi, J. M., and K. B. Baker (1998), Large-scale imaging of high-latitude convection with Super Dual Auroral Radar Network HF radar observations, *J. Geophys. Res.*, *103*(A9), 20,797–20,811, doi:10.1029/98JA01288.

Ruohoniemi, J. M., and R. A. Greenwald (1996), Statistical patterns of high-latitude convection obtained from Goose Bay HF radar observations, *J. Geophys. Res.*, *101*(A10), 21,743–21,764, doi:10.1029/96JA01584.

Ruohoniemi, J. M., and R. a. Greenwald (1998), The response of high-latitude convection to a sudden southward IMF turning, *Geophys. Res. Lett.*, *25*(15), 2913–2916, doi:10.1029/98GL02212.

Ruohoniemi, J. M., and R. A. Greenwald (2005), Dependencies of high-latitude plasma convection: Consideration of interplanetary magnetic field, seasonal, and universal time factors in statistical patterns, *J. Geophys. Res.*, *110*, A09204, doi:10.1029/2004JA010815.

Sergeev, V. A., E. M. Sazhina, N. A. Tsyganenko, J. A. Lundblad, and F. Soraas (1983), Pitch-angle scattering of energetic protons in the magnetotail current sheet as the dominant source of their isotropic precipitation into the nightside ionosphere, *Planet. Space Sci.*, *31*(10), 1147–1155, doi:10.1016/0032-0633(83)90103-4.

Shukhtina, M. A., and S. E. Milan, (2014), ECLAT system level data product report (D430.1), *Tech. Rep.*

Siscoe, G. L., and T. S. Huang (1985), Polar cap inflation and deflation, *J. Geophys. Res.*, *90*(A1), 543–547.

Stern, D. P. (1975), The motion of a proton in the equatorial magnetosphere, *J. Geophys. Res.*, *80*(4), 595–599, doi:10.1029/JA080i004p00595.

Volland, H. (1978), A model of the magnetospheric electric convection field, *J. Geophys. Res.*, *83*(A6), 2695–2699, doi:10.1029/JA083iA06p02695.

Walach, M.-T., and S. E. Milan (2015), Are steady magnetospheric convection events prolonged substorms?, *J. Geophys. Res. Space Physics*, *120*, 2695–2699, doi:10.1002/2014JA020631.

Xu, L., A. V. Koustov, J. Thayer, and M. A. Mccready (2001), SuperDARN convection and Sondrestrom plasma drift, *Ann. Geophys.*, *19*(7), 749–759.

Xu, L., A. V. Koustov, J. Xu, R. Drayton, and L. Huo (2008), A 2-D comparison of ionospheric convection derived from SuperDARN and DMSP measurements, *Adv. Space Res.*, *42*(7), 1259–1266, doi:10.1016/j.asr.2007.06.044.